ChemPubSoc Europe

DOI: 10.1002/chem.201304202

CHEMISTRY A European Journal Full Paper

Photosensitizers

Photodynamic Therapy Efficacy Enhanced by Dynamics: The Role of Charge Transfer and Photostability in the Selection of Photosensitizers

Luis G. Arnaut,*[a, b] Mariette M. Pereira,[a] Janusz M. Dąbrowski,*[c] Elsa F. F. Silva,[a] Fábio A. Schaberle,[b] Artur R. Abreu,[b] Luís B. Rocha,[d] Madalina M. Barsan,[a] Krystyna Urbańska,[e] Grażyna Stochel,[c] and Christopher M. A. Brett[a]

Abstract: Progress in the photodynamic therapy (PDT) of cancer should benefit from a rationale to predict the most efficient of a series of photosensitizers that strongly absorb light in the phototherapeutic window (650–800 nm) and efficiently generate reactive oxygen species (ROS = singlet oxygen and oxygen-centered radicals). We show that the ratios between the triplet photosensitizer–O_2 interaction rate constant (k_D) and the photosensitizer decomposition rate constant (k_d), k_D/k_d, determine the relative photodynamic activities of photosensitizers against various cancer cells. The same efficacy trend is observed in vivo with DBA/2 mice bearing S91 melanoma tumors. The PDT efficacy intimately depends on the dynamics of photosensitizer–oxygen interactions: charge transfer to molecular oxygen with generation of both singlet oxygen and superoxide ion (high k_D) must be tempered by photostability (low k_d). These properties depend on the oxidation potential of the photosensitizer and are suitably combined in a new fluorinated sulfonamide bacteriochlorin, motivated by the rationale.

Introduction

Photodynamic therapy (PDT) combines light, a photosensitizer, and oxygen to generate reactive oxygen species (ROS: singlet oxygen and oxygen-centered radicals) and destroy targeted tissue.[1] PDT is progressively becoming a credible alternative to surgery, chemotherapy, and radiotherapy in the management of cancer because it can be repeated many times in the same site and has no long-term side effects.[2] The directionality of laser light, the eventual affinity of photosensitizers towards tumors, and the short diffusion radius of the ROS minimize damage to healthy tissues. Moreover, the oxidative stress induced by these ROS triggers the local destruction of the tumor, whereas the local inflammation resulting from PDT activates antitumor immune responses capable of causing regression in distant tumors and induce long-term immune memory.[3] Although a handful of photosensitizers are currently used for various indications,[4] the realization of the full potential of PDT still awaits the development of more efficient photosensitizers with reduced skin photosensitivity after treatment.

Various authors have discussed photosensitizer properties critical to the success of PDT.[5] Generally accepted properties are low dark toxicity, amphiphilicity, selectivity towards tumor tissue, simple formulation, long shelf-life, rapid clearance from the body, facile synthesis, feasible scaleup, $700\ nm < \lambda_{max} < 800\ nm$, $\varepsilon_{infrared} > 10^5\ M^{-1}\ cm^{-1}$, $\Phi_F \geq 0.2$, $\Phi_T \geq 0.7$, triplet lifetime $\tau_T \geq 100\ \mu s$, $\Phi_\Delta > 0.5$, and $\Phi_{pd} < 10^{-5}$, in which Φ refers to quantum yields of fluorescence (F), triplet (T), singlet oxygen (Δ), and photodecomposition (pd). Singlet oxygen is generated by energy transfer from the photosensitizer triplet state to molecular oxygen (type II reaction), but the triplet state of the photosensitizer may also participate in electron or hydrogen-atom transfer reactions (type I reaction) that eventually lead to oxygen-centered radicals.[6] Interestingly, charge-transfer interactions between the triplet state of the photosensitizer and molecular oxygen facilitate the generation of the superoxide ion and the hydroxyl radical, in addition to singlet oxygen, and increase phototoxicity.[5e,7] Moreover, the localization of the

[a] Prof. L. G. Arnaut, Prof. M. M. Pereira, E. F. F. Silva, Dr. M. M. Barsan, Prof. C. M. A. Brett
Chemistry Department, University of Coimbra
3004-535 Coimbra (Portugal)
Fax: (+351) 239-827-703
E-mail: lgarnaut@ci.uc.pt

[b] Prof. L. G. Arnaut, Dr. F. A. Schaberle, Dr. A. R. Abreu
Luzitin SA, Ed. Bluepharma, S. Martinho do Bispo
3045-016 Coimbra (Portugal)

[c] Dr. J. M. Dąbrowski, Prof. G. Stochel
Faculty of Chemistry, Jagiellonian University
30-060 Krakow (Poland)
E-mail: jdabrows@chemia.uj.edu.pl

[d] L. B. Rocha
Bluepharma SA, Ed. Bluepharma, S. Martinho do Bispo
3045-016 Coimbra (Portugal)

[e] Prof. K. Urbańska
Faculty of Biochemistry, Biophysics and Biotechnology
Jagiellonian University, 30-387 Krakow (Poland)

Supporting information for this article is available on the WWW under http://dx.doi.org/10.1002/chem.201304202.

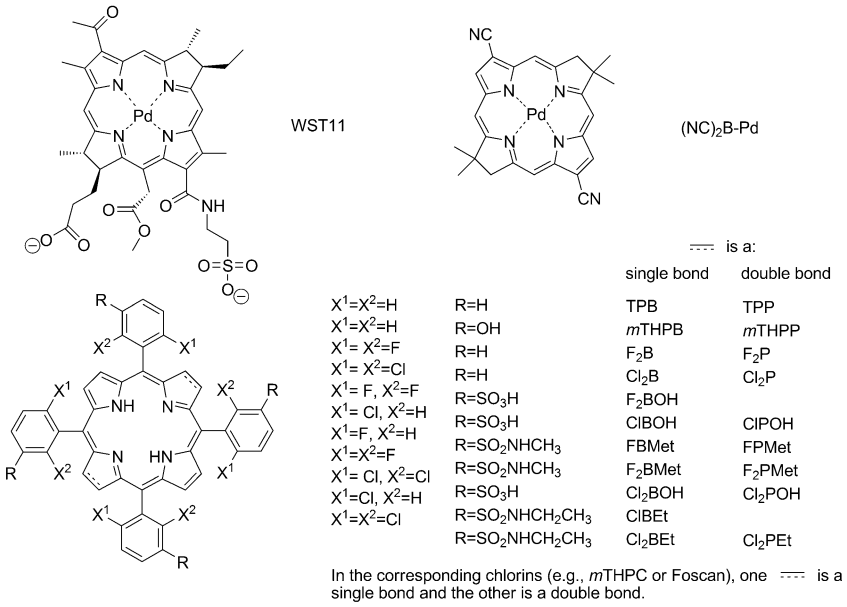

Scheme 1. Promising bacteriochlorin photosensitizers and the general structures of photosensitizers discussed in this study.

photosensitizer in the endoplasmic reticulum (ER) and its ability to generate strong ROS-dependent ER stress was shown to induce immunogenic cancer cell death.[8]

Current efforts to make the "ideal photosensitizer" focus on bacteriochlorins because they intrinsically have some of the desired properties mentioned above.[9] Scheme 1 illustrates bacteriochlorins currently investigated and our own halogenated tetraphenylbacteriochlorins.[10] The use of naturally occurring bacterichlorins, or their derivatives such as WST11, is very appealing and substantiated by interesting results,[11] but their (photo and thermal) stability is less than ideal. Alternatively, de novo synthesis of more stable bacteriochlorins such as $(NC)_2B$–Pd is now a well-established multistep route capable of generating a wide range of bacteriochlorins with tunable properties.[12] Our focus on halogenated tetraphenylbacteriochlorins was motivated by the ability to synthesize a wide variety of porphyrin precursors in two to three steps followed by the one-step reduction to the corresponding bacteriochlorin in the absence of solvents,[10,13] and by their stability,[10,14] strong absorption in the near-infrared region, efficient generation of ROS,[15] ER localization, and favorable biodistribution.[7,16]

Access to a vast library of compounds with therapeutic potential is a critical step in the discovery of new drugs. However, the potential of the therapy can only be fully exploited with a rationale that uses observable properties to anticipate the best drug candidate. Structure–activity relationships have been notoriously difficult to establish for PDT photosensitizers. Hamblin, Lindsey, and co-workers reported that 10 J cm^{-2} at 732 nm required 0.1 μM of a bacteriochlorin with $\log P_{OW} = 2.3$ to kill 50% of HeLa cells but a related bacteriochlorin with $\log P_{OW} = 1.4$ required 4 μM.[9c] Pandey and co-workers provided examples of phototoxicities of ketobacteriochlorins towards Colon26 cells differing by more than one order of magnitude with subtle changes in structure.[17] We also showed that the photodynamic effect in vitro is not simply correlated with any of the properties judged critical to the success of PDT,[7] and that tumor growth delays in animal models are very sensitive to subtle changes in properties (27 days for ClBOH[16b] to 44 days for Cl_2BEt).[16c] This work discloses illuminating dependences of PDT efficacy on the dynamics of the charge transfer between the photosensitizer and oxygen (which determine the nature of the ROS generated), and on the stability of the photosensitizer (which determines its throughput). These dependences are expected to be ubiquitous phenomena affecting the performance of all photosensitizers and provide the grounds to predict the most efficient of a family of photosensitizers. The rationale derived by these dependences motivated the detailed investigation of a new fluorinated sulfonamide bacteriochlorin for PDT of cancer (F_2BMet, Scheme 1).

Results

Synthesis

The synthesis was oriented by the requirements of simplicity, feasibility of scaleup, and ability to offer a variety of stable bacteriochlorins. The synthesis of *ortho*-halogenated phenyl porphyrins using the nitrobenzene method,[18] with the modulation of their amphiphilicity by means of chlorosulfonation followed by reaction with nucleophiles,[19] led to the desired halogenated sulfonamide porphyrins.[20] We selected the solvent-free diimide hydrogenation method (Scheme 2) to obtain the bacteriochlorins in view of its simplicity and functional-group tolerance.[13] Details of the synthesis are given in the Experimental Section.

Photophysics and photochemistry

Table 1 presents the absorption, fluorescence, and triplet properties of tetraphenylporphyrin derivatives and Photofrin (a mixture of hematoporphyrin derivatives for injection, approved for clinical use) taken from the literature, and new data on F_2PMet and F_2BMet. F_2BMet was synthesized in this work to meet the requirements of photostability and large charge-transfer interactions with oxygen. F_2BMet has $\varepsilon_{743} = 140\,000\ M^{-1}cm^{-1}$ in ethanol (Figure 1) and the Beer–Lambert law is followed in the micromolar range. The molar absorption coefficient is based on the chromatographic content of the sample and it is larger

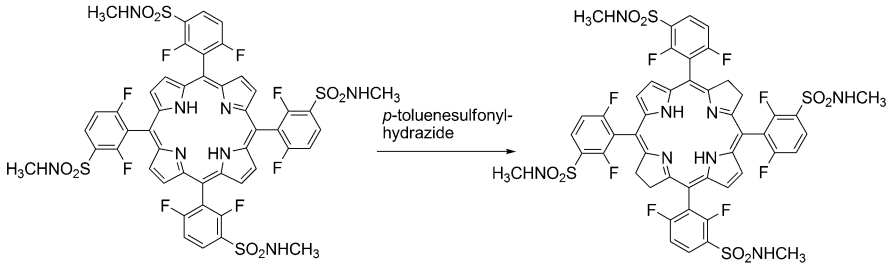

Scheme 2. One-step synthesis of F_2BMet from F_2PMet without using solvents or bases.

than those of related bacteriochlorins in Table 1 (e.g., Cl_2BEt) because earlier corrections only accounted for chlorin impurities.[10] However, this ε_{743} is in excellent agreement with those of halogenated tetraphenylbacteriochlorins purified by preparative thin-layer chromatography.[14a]

The fluorescence quantum yield of chlorinated tetraphenylbacteriochlorins is very low (Cl_2BEt, $\Phi_F = 0.013$),[23a] as expected from the internal heavy-atom effect,[21b] but the analogous fluorinated bacteriochlorin has an intense fluorescence (F_2BMet, $\Phi_F = 0.138 \pm 0.011$) that may provide guidance for the location of the tumor tissue during therapy. The Supporting Information presents the 3.0 ns fluorescence decay at 765 nm measured by single-photon counting with excitation at 378 nm, and its fitting to a monoexponential function.

Figure 1 also presents the transient absorption spectrum and decays of solutions of F_2BMet in ethanol. The monoexponential decays give triplet lifetimes of $\tau_T^0 = 47$ μs and $\tau_T = 216$ or 50 ns in nitrogen-, air-, or oxygen-saturated solutions, respectively. The bleaching of the ground-state absorption of F_2BMet at 745 nm recovers almost quantitatively and was used to calculate the triplet molar absorption coefficient at 790 nm ($\varepsilon_T = 55\,000\ M^{-1}cm^{-1}$), which was then used to obtain the triplet quantum yield, $\Phi_T = 0.65 \pm 0.10$, by employing benzophenone as reference.

Time-resolved photoacoustic calorimetry (PAC)[15,21a] was used to measure the heat released after pulsed-laser excitation of the bacteriochlorin. Deconvolution of the PAC signals using

Table 1. Data for halogenated sulfonamide porphyrin derivatives in ethanol or methanol, and of halogenated porphyrin derivatives in toluene, compared with those of tetra(3-hydroxyphenyl)porphyrin derivatives and Photofrin, and photodegradation in PBS/methanol.

	Absorption		Fluorescence			Triplet				Redox potentials (vs SCE)			
	λ_{max} [nm]	$\varepsilon_{max}\times10^3$ [$M^{-1}cm^{-1}$]	λ_{max} [nm]	Φ_F	τ_F [ns]	Φ_T	τ_T [ns]	$k_q\times10^9$ [$M^{-1}s^{-1}$]	Φ_Δ	E^0_{red1} [V]	$E^{0\,[a]}_{ox}$ [V]	E^0_{ox1} [V]	$\Phi_{pd}\times10^{-6}$
TPP[b]	650	9.6	652	0.10	10.6	0.73	349	1.6	0.71	−1.08	–	0.95	–
F_2P[b]	655	5.3	657	0.069	–	≈0.89	493	1.1	0.84	–	–	1.23[d]	–
FPMet[c]	639	0.79	644	0.096	14.6	–	309	1.5	0.60	–	–	–	–
F_2PMet	639	0.68	654	0.049	–	0.71	389	1.2	0.71	–	–	–	–
ClPOH[e]	633	0.50	640	0.008	–	–	720	0.66	0.74	–	0.70	1.28	10
Cl_2POH[c]	–	–	–	–	–	–	855	0.56	1.00	–	–	–	–
Cl_2P[b]	660	2.1	661	0.005	0.66	≈1	641	0.87	0.98	–	–	1.23[d]	–
Cl_2PEt[c]	646	0.61	655	0.002	0.26, 0.77	≈1	710	0.67	0.85	−0.94	0.85	1.38	7
TPC[b,f]	651	42	–	–	–	–	–	–	–	−1.12	–	0.88	–
F_2C[b]	655	40	658	0.124	–	≈0.88	305	1.8	0.88	–	–	–	–
FCMet[c]	652	34	657	0.396	–	–	285	–	0.58	–	–	–	–
F_2CMet[c]	655	50	657	0.36	–	0.58	283	1.7	0.54	–	–	–	2[g]
Cl_2C[b]	660	2.1	661	0.005	–	≈1	393	1.4	0.98	–	–	–	–
Cl_2CEt[c]	658	29	662	0.028	0.24, 0.53	–	–	–	–	−0.84	0.85	1.36	–
FBMet[c]	741	62	745	0.129	3.6	–	200	2.4	0.63	–	–	–	–
TPB[b,f]	742	120	–	–	–	–	–	–	–	−1.10	–	0.40	–
F_2B[b]	744	140	745	0.068	3.8	≈0.81	216	2.6	0.48	−0.95	–	0.65	–
F_2BOH[c]	745	56	745	0.023	–	–	268	–	0.44	−0.93	0.55	0.70	203[h]
F_2BMet	743	140	746	0.138	3.0	0.65	216	2.2	0.43	−0.74	0.80	0.80	10
ClBOH[c]	742	61	745	0.040	–	–	246	1.9	0.42	–	–	–	300
Cl_2BOH[c]	745	61	748	0.006	–	–	226	2.1	0.85	–	–	–	–
Cl_2B[b]	747	126	748	0.012	–	≈1	254	2.1	0.60	–	–	–	–
ClBEt[c]	743	76	746	0.038	–	–	228	2.1	0.61	–	–	–	–
Cl_2BEt[c]	745	110	747	0.013	0.39, 0.54	≈1	265	1.8	0.66	−0.79	0.82	0.82	6
*m*THPB[i]	735	91	746	0.11	–	0.83	–	2.5	0.43	–	–	–	3.8
*m*THPC[i]	650	29.6	653	0.089	–	0.89	–	1.8	0.43	–	–	–	33
*m*THPP[i]	644	3.4	649	0.12	–	0.69	–	1.9	0.46	–	–	–	1500
Photofrin[j]	630	1.17	–	–	–	0.8	–	1.5	0.36	–	–	–	55

[a] Oxidations assigned to $PhSO_2NHR$ or $PhSO_3H$ groups; $E_{red} = -0.27$ V found for F_2BOH is also assigned to the $PhSO_3H$ group. [b] Refs. [14a, 18, 21], with oxidation potentials in CH_2Cl_2 and reduction potentials in DMF vs SCE from Ref. [22]. [c] Partly from Refs. [7, 10, 15, 23]. [d] Oxidation potentials in benzonitrile in Ref. [24] corrected for the difference of oxidation potentials for that study and in Ref. [22]. [e] Partly from Refs. [20, 25]. [f] From Ref. [26]. [g] In H_2O/MeOH, 2:3 v/v. [h] In PBS, but for ClBOH Φ_{pd} changes only from 2.8×10^{-4} in PBS to 3.0×10^{-4} in PBS/MeOH. [i] In methanol from Refs. [27, 28]. [j] Φ_Δ refers to 10 μM hematoporphyrin derivative in PBS (Ref. [29]).

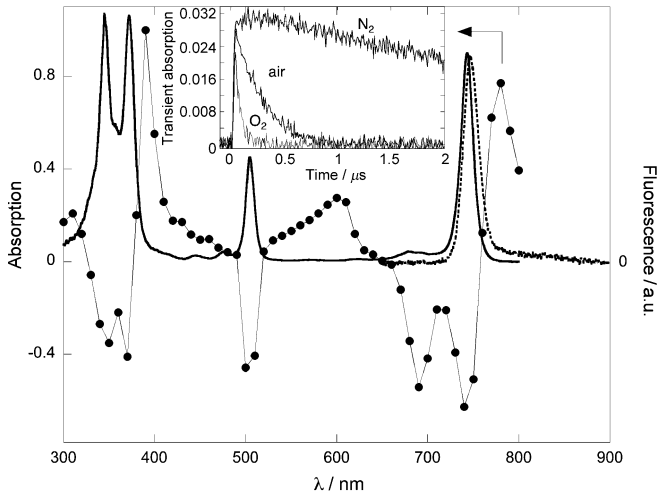

Figure 1. F_2BMet absorption (solid line, 6.5 μM) and fluorescence (dotted line, $\lambda_{exc}=735$ nm) and transient absorption (line and circles, collected 30 ns after the laser pulse) in ethanol. Inset: decays at 780 nm in nitrogen-, air-, or oxygen-saturated ethanol measured by laser flash photolysis at 20 °C with $\lambda_{exc}=355$ nm.

a photoacoustic reference gives the energy released first in the formation of the triplet and then in the decay of the triplet.[30] The fast heat released was used together with $\Phi_T=0.65\pm0.10$ to obtain the triplet-state energy of F_2BMet as $E_T=(26\pm2)$ kcal mol^{-1}. The second heat release in the presence of oxygen was used together with the energy and quantum yield of singlet oxygen to obtain the energy stored in other ROS, $\Phi_{CT}E_{CT}=(4.5\pm0.6)$ kcal mol^{-1}, in which E_{CT} is the energy of the charge-separated state generated by electron transfer from F_2BMet to molecular oxygen and Φ_{CT} is the corresponding quantum yield. Details are given in the Supporting Information.

Reactive oxygen species

Excitation of bacteriochlorins at 355 nm in ethanol generates singlet oxygen with its characteristic phosphorescence at 1270 nm with a lifetime of approximately 14 μs. The singlet-oxygen quantum yields were obtained by using the phosphorescence intensities according to a previously described procedure.[15] Representative data are presented in the Supporting Information. Evidence for the photogeneration of other ROS, such as $O_2^{-\bullet}$ and $OH^{\bullet}$, has been obtained in DMSO and phosphate-buffered saline (PBS) solution using 5,5-dimethyl-1-pyrroline *N*-oxide (DMPO) as spin trap to form DMPO–OOH and DMPO–OH radical adducts while irradiating bacteriochlorins, and EPR to identify such adducts.[15] The Supporting Information presents similar evidence obtained with the irradiation of F_2BMet. In the presence of 30 μg mL^{-1} catalase or of 50 μg mL^{-1} superoxide dismutase, the DMPO–OH signal disappeared completely. These findings corroborate our mechanism of hydroxyl radical formation in aqueous solution as a sequence of steps involving the superoxide ion and hydrogen peroxide.[15] Moreover, after the addition of NaN_3 (5 mM), a singlet-oxygen inhibitor, we still observe the DMPO–OH EPR signal, which indicates that singlet oxygen is not involved in the formation of $OH^{\bullet}$ by F_2BMet.

Electrochemistry

Cyclic voltammograms were recorded at slow sweep rates, 25 mV s^{-1}, in acetonitrile or dichloroethane containing 0.1 M tetra-*n*-butylammonium perchlorate. Figure 2 presents typical cyclic voltammetric responses of sulfonamide porphyrin derivatives. Table 1 lists the lowest redox potentials measured in this work. E_{red1} and E_{ox1} refer to the macrocycle and E_{ox} to the sulfonic or sulfonamide groups.

The bacteriochlorins investigated, excepting F_2BOH, undergo two reversible reductions at $E_{red1}=-0.74$ to -0.95 V versus a saturated calomel electrode (SCE) and $E_{red2}=-1.15$ to -1.46 V versus SCE, respectively, to form the radical anion and dianion. Two reversible oxidations were also recorded at $E_{ox1}=$ 0.65–0.82 V versus SCE and $E_{ox2}=1.18$–1.24 V versus SCE, which correspond to the formation of the radical cation and dication. The first oxidation is reversible, whereas the second one is quasi-reversible or irreversible owing to the instability of the dication generated.[31] F_2BOH presents three irreversible oxidations, the third one occurring at a less positive potential of $+0.55$ V and the corresponding reduction at -0.27 V versus SCE, which correlated with the oxidation and reduction of the Ph–SO_3H group.

The presence of the sulfonamide electron-withdrawing group in the phenyl ring increases the first oxidation potential

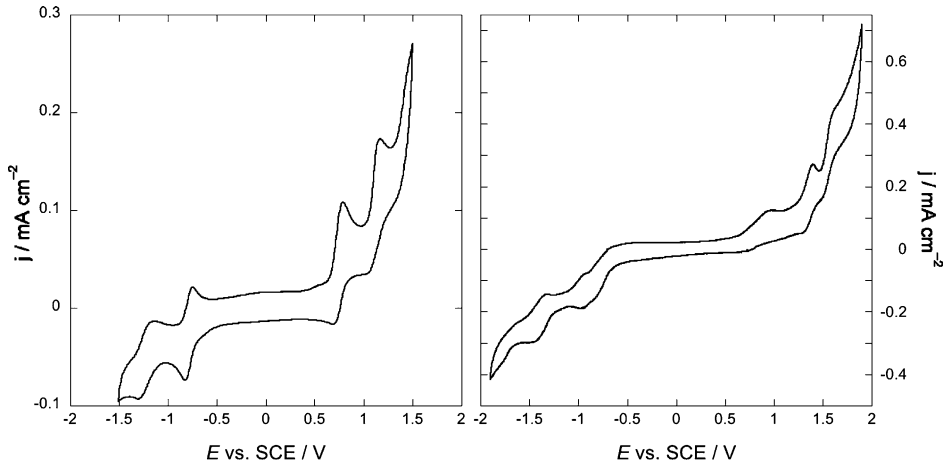

Figure 2. Left panel: cyclic voltammogram recorded in 0.1 M TBAP dissolved in CH_3CN containing 0.5 mM F_2BMet; scan rate 25 mV s^{-1}. Right panel: cyclic voltammogram recorded in 0.1 M TBAP dissolved in CH_3CN containing 0.5 mM Cl_2PEt; scan rate 25 mV s^{-1}.

from +0.65 in F_2B to +0.80 in F_2BMet and to +0.82 in Cl_2BEt. Cl_2PEt and Cl_2CEt exhibited similar cyclic voltammetric responses, characterized by two reversible reductions and three oxidations. The third oxidation wave at less positive potentials, of approximately +0.85 V versus SCE, is related to irreversible sulfonamide oxidation, visible in the case of porphyrins and chlorins, in which the first oxidation of the macrocycle occurs at more positive potentials, +1.38 and +1.36 V versus SCE, for Cl_2PEt and Cl_2CEt, respectively. Similar oxidation potential values corresponding to sulfonamide have been reported for sulfadiazine[32] and sulfaguanidine.[33] The oxidation of the sulfonamide group overlaps with the first oxidation of the macrocycle, located at +0.80 and +0.82 V versus SCE for F_2BMet and Cl_2BEt, respectively. ClPOH, which contains the same $-SO_3H$ group as F_2BOH, presents three irreversible oxidation processes, with the less positive potential being $-SO_3H$ oxidation, at +0.70 V versus SCE. The oxidation of the $-SO_3H$ group occurs at lower potentials than that of the sulfonamide $-SO_2NHR$ group.

The potential difference, ΔE, between the first oxidation and first reduction couples, $\Delta E_{ox1-red1}$, decreases in the order porphyrin > chlorins > bacteriochlorins, with values of 2.32, 2.20, and approximately 1.57 V versus SCE, respectively. The assignment of the oxidation and reduction potentials is consistent by the correlation between $E^0_{ox1}-E^0_{red1}$ and the singlet-state energy (E_S) of these macrocycles.[9d]

The energy of the full electron transfer from the photosensitizer to molecular oxygen is given by $\Delta G_{CT}=E^*_{ox}-E^A_{red}$, in which $E^*_{ox}=E^D_{ox1}-E_T$ is the triplet-state oxidation potential, and the half-wave reduction potential of oxygen is $E^A_{red}=-0.78$ V versus SCE in DMSO,[34] or −0.425 V versus SCE in hydrogen-bonding solvents.[35] This latter value is more relevant for biological reactions and for the determination of ΔG_{CT} in ethanol. The ΔG_{CT} values used in this work were calculated with $E^A_{red}=-0.425$ V versus SCE. For F_2BMet we calculate $\Delta G_{CT}=(2\pm 2)$ kcal mol^{-1} ($\Delta E_{CT}=28.2$ kcal mol^{-1} and $\Phi_{CT}=0.16\pm0.02$).

Photodecomposition

The photostability of a photosensitizer (S) is best described by its photodecomposition quantum yield (Φ_{pd}), which is defined as the ratio between the rate of disappearance of photosensitizer molecules and the rate of absorption of photons as shown in Equation (1):

$$\Phi_{pd} = v_d/v_p \quad (1)$$

in which v_d and v_p are defined by Equations (2) and (3), respectively:

$$v_d = \frac{dn}{dt} = \frac{V_{irr}N_A}{\varepsilon l}\frac{dA}{dt} = k_d[S] \quad (2)$$

$$v_p = \frac{\lambda P}{hc}(1-10^{-A}) \quad (3)$$

and k_d is the decomposition rate constant, P the power of the monochromatic incident light absorbed in the volume (V_{irr}) by a solution of absorbance A. Table 1 shows published Φ_{pd} values of some halogenated bacteriochlorins,[10] together with additional data obtained in aerated solvents for F_2BMet (laser irradiation at 748 nm) and for halogenated sulfonamide porphyrins and chlorins (pulsed-laser excitation at 508 or 653 nm, respectively). The similar Φ_{pd} values of Cl_2PEt, Cl_2CEt, and Cl_2BEt is readily explained in terms of their lowest oxidation potentials. The irreversible oxidation of the sulfonamide group and reversible oxidation of the bacteriochlorin macrocycle, which occur at very similar oxidation potentials, control the decomposition rate.

Free-energy relationships

The triplet-state quenching rate constant is given by Equation (4):

$$k_q = (1/\tau_T - 1/\tau_T^0)/[O_2] \quad (4)$$

but residual oxygen in N_2-saturated solutions leads to underestimates of τ_T^0 in organic solvents in which $\tau_T^0 > 30$ μs. In such cases, it is more appropriate to calculate the triplet-state quenching rate constant as $k_q=1/(\tau_T[O_2])$. The rate constants presented in Table 1 were calculated with this equation and the concentration of oxygen in the solvent of the experiment. Figure 3 presents the dependence of k_q on ΔG_{CT} and of Φ_{pd} on the lowest E_{ox}. The E_{ox1} of THPP, THPC, and THPB were taken from TPP, TPC, and TPB, respectively.

In the absence of charge transfer in the {sensitizer···O_2} encounter complex, spin statistics limit k_q to one ninth of the diffusion rate constant ($k_{diff}=9.5\times10^9$ M^{-1} s^{-1} in ethanol).[23b] How-

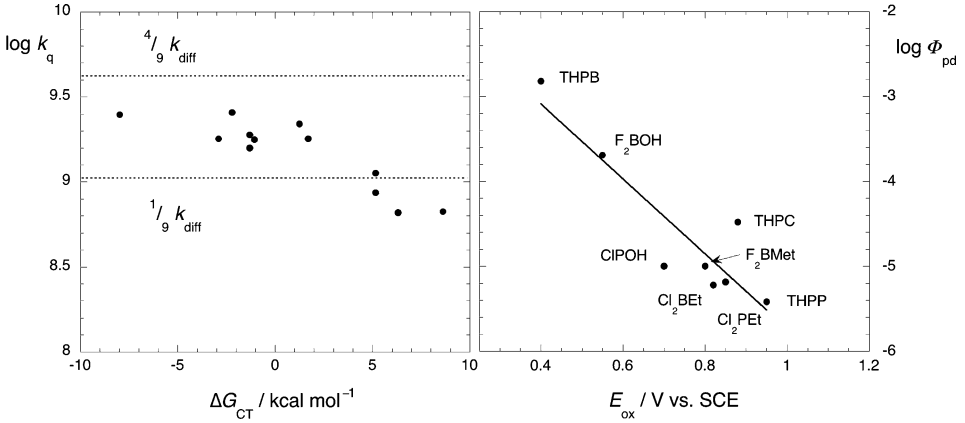

Figure 3. Dependence of the triplet-quenching rate constant (k_q) and photodegradation quantum yield (Φ_{pd}) of tetraphenylporphyrin derivatives on their electron-donor abilities, represented by the free energy for electron transfer to oxygen or by their lowest oxidation potential.

ever, the rate constant of charge-transfer-assisted quenching of porphyrin derivatives by molecular oxygen increases with the free energy of the reaction and should approach $^4/_9\,k_{diff}$.[15,36] Bacteriochlorins show $k_q > {}^1/_9\,k_{diff}$ and $\Phi_\Delta < 1$, which are the hallmarks of charge-transfer interactions between a photosensitizer and molecular oxygen.[15,37] Thus, the dependence of k_q on ΔG_{CT} can be regarded as a free-energy relationship. In hydrogen-bonding solvents, the $-\Delta G_{CT}$-driven charge-transfer dynamics increase the formation of superoxide ion. FBMet, F_2BMet, ClBEt, and *m*THPB exhibit $k_q > 2\times 10^9\,M^{-1}s^{-1}$ and are good examples of photosensitizers that take advantage of this effect.

Φ_{pd} is a measure of the decomposition rate constant (k_d) under constant power of absorbed light (P). The photodecomposition products of bacteriochlorins and chlorins are oxidation products and, therefore, the dependence of Φ_{pd} (or k_d) on E_{ox} is also a free-energy relationship. The condition of photostability ($\Phi_{pd} < 10^{-5}$) requires $E_{ox} > 0.7$ V versus SCE, which is met by F_2BMet and Cl_2BEt in Table 1.

These two free-energy relationships show that strong charge transfer to molecular oxygen (high k_q) and high photostability (low Φ_{pd}) are singularly combined in F_2BMet. It should be emphasized that the solubility of oxygen decreases from organic solvents ($[O_2]_{ethanol} = 2.1$ mM, $[O_2]_{toluene} = 1.8$ mM)[38] to water ($[O_2]_{aq} = 0.29$ mM at 20 °C), and that the oxygen partial pressure decreases from $pO_2 = 150$ mm Hg for cell cultures to 14 mm Hg in the blood vessels and to 5 mm Hg some 70–80 μm away from the closest blood vessel.[39] Thus, the kinetics of the interaction between the photosensitizer triplet state and oxygen assumes an even greater relevance in vivo. The photobleaching of photosensitizers in biological media is also severe, and we can expect the high k_q and low Φ_{pd} of F_2BMet to be most valuable for PDT. This motivated additional work to characterize the biological activity of F_2BMet.

In vitro studies

Intracellular localization was investigated in A549 cells co-incubated with F_2BMet and fluorescent probes specific for lysosomes, mitochondria, or endoplasmic reticulum. Figure 4 shows the overlaid images, with the fluorescence of F_2BMet in red and that of the organelle-specific probes in green. The topographic profiles of F_2BMet reveal a high degree of localization in the ER, some in the mitochondria, and none in the lysosomes, which is consistent with those of other halogenated sulfonamide bacteriochlorins.[7]

F_2BMet was also co-incubated with 3′-(*p*-aminophenyl)fluorescein (APF), because this probe reacts rather selectively with the hydroxyl radical to release fluorescein that has a characteristic fluorescence near 520 nm.[40] Figure 5 shows the fluorescence of F_2BMet in cells and the fluorescence of fluorescein observed after the illumination of one cell at 514 nm with the argon laser of the confocal microscope. The argon laser was controlled to illuminate only one cell, and only this cell showed fluorescein emission. The $OH^\bullet$ radical formed upon illumination of F_2BMet in vitro reacts locally with APF and leads to the fluorescein emission. The Supporting Information presents the case of the illumination of the whole cell culture with a diode laser at 750 nm.

Photocytotoxicity

Incubation of A549 and S91-I3 cells for 20 h with F_2BMet in the 0.5–25 μM concentration range, or of CT26 and HT-29 with up

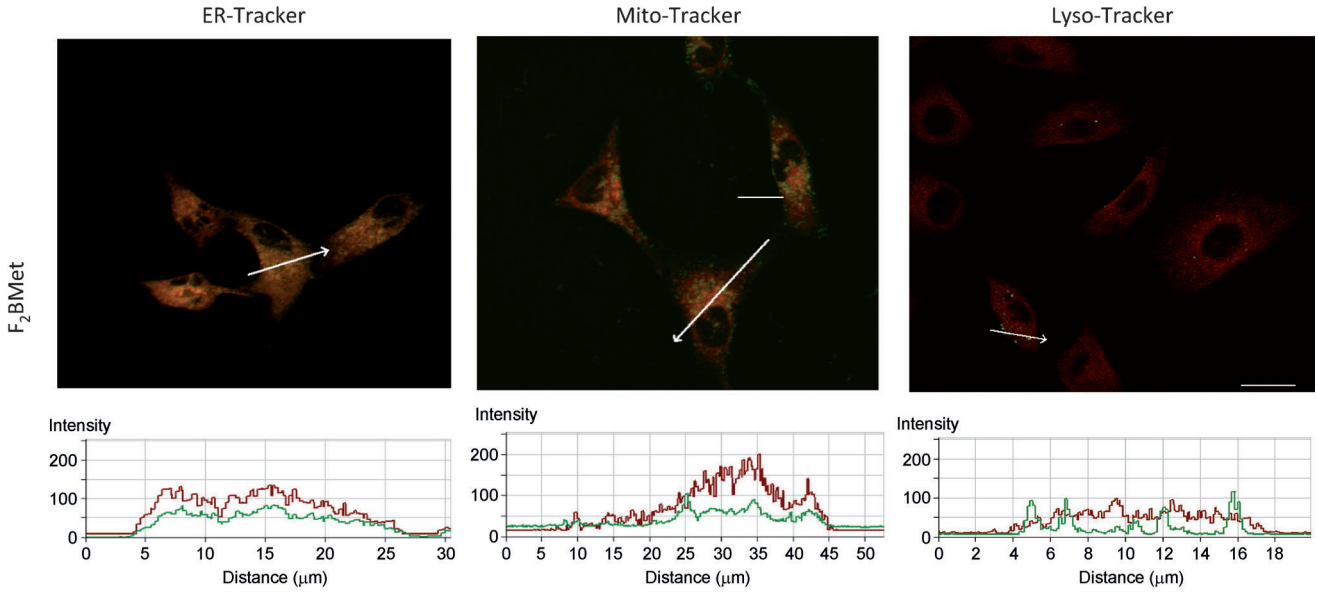

Figure 4. Fluorescence micrographs of A549 cells showing intracellular localization of F_2BMet evaluated by confocal microscopy. Cells were marked with dyes for endoplasmic reticulum (ER-Tracker Green, left), mitochondria (Mito-Tracker Green, center), and lysosomes (LysoTracker Green, right). Intracellular distribution was studied by fluorescence with appropriate selection of emission wavelengths. For each image, a profile of fluorescence intensity along the white arrow is shown. The green topographic profile corresponds to the emission of the tracker and the red profile to the photosensitizer emission.

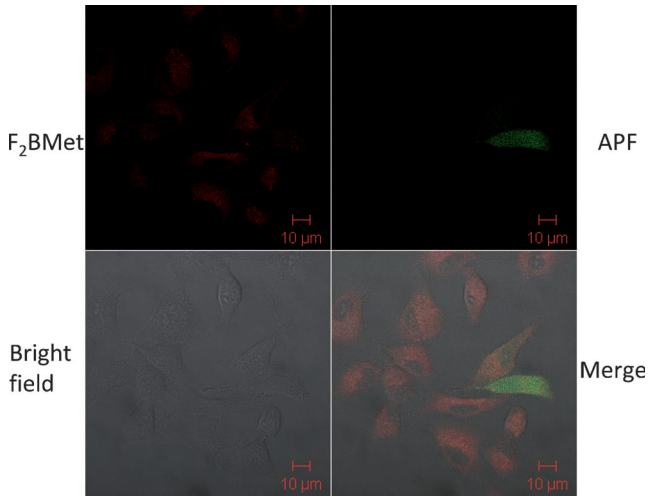

Figure 5. Fluorescence micrographs of A549 cells co-incubated with F_2BMet and APF showing the red fluorescence from the photosensitizer (upper left) and the green fluorescence from fluorescein after illumination at 514 nm with the argon laser of the confocal microscope just on a single cell (upper right), the overlaid micrographs (lower right), and the bright-field image (lower left).

to 200 μM F_2BMet did not reveal any significant cytotoxicity. We selected [F_2BMet] = 5 μM for the phototoxicity studies with broadband irradiation because this dose leads to an accumulation of F_2BMet in A549 and S91-I3 cells comparable to that of related bacteriochlorins.[7] The filtered halogen lamp has a relatively homogeneous power spectrum in the spectral region between 630 and 800 nm, and is useful to compare the phototoxicity of different photosensitizers. Table 2 presents the lethal light dose required to kill 50 (LLD_{50}) or 90% (LLD_{90}) of the cells in the culture, respectively, calculated from data at different light doses. F_2BMet is the most phototoxic photosensitizer.

Table 3 presents the photosensitizer concentrations required to kill 50 or 90% of A549, CT26, PC-3, and HT-29 cells, LD_{50} or LD_{90}, under laser-light doses of 1 and 6 J cm^{-2}. Additionally, we made a direct comparison between the dark cytotoxicities of F_2BMet, *m*THPC, and Photofrin, and their phototoxicities under 1 J cm^{-2} and 8 mW cm^{-2} irradiation using CT26 and HT-29 cell lines. These cell lines were incubated with the maximum concentration of F_2BMet, *m*THPC, or Photofrin below the onset of their dark cytotoxicity and were irradiated with varying laser-light doses at 748, 652, and 633 nm, respectively. The low dark cytotoxicity of F_2BMet allows for the use of higher concentrations and the opposite is true for *m*THPC. Figure 6 shows the resulting phototoxicities.

Table 2. Light doses, under filtered halogen lamp illumination, required to kill 50 or 90% of A549 and S91-I3 cells in vitro after 24 h of incubation with the photosensitizers.[a]

	Log P_{OW}	Onset dark toxicity [μM]	LLD_{50} [J cm^{-2}]		LLD_{90} [J cm^{-2}]	
			A549	S91-I3	A549	S91-I3
ClPOH	−2.7	200	–	1.0	–	4.0
ClBOH	−1.7	>200	–	0.13	–	0.26
ClBEt	2.5	–	0.16	0.05	0.29	0.22
Cl_2BEt	1.8	–	0.13	0.05	0.25	0.19
FBMet	2.7	–	0.053	0.04	0.22	0.17
F_2BMet	1.9	>100	0.045	0.03	0.16	0.14
Photofrin	0.9	25	–	0.05	–	0.18

[a] Data on ClPOH from Ref. [29a], on ClBOH, ClBEt, Cl_2BEt, and FBMet from Refs. [7,19a], and on Photofrin from Ref. [41] with its P_{OW} at pH 7 from Ref. [42]. ClPOH was incubated at a concentration of 20 μM, Photofrin at 17 μM, and the bacteriochlorins at 5 μM.

Biodistribution and pharmacokinetics

The biodistribution and pharmacokinetics of F_2BMet were studied after intravenous (i.v.) injection in the tail vein of DBA/2 mice.

Groups of three or four animals were sacrificed at different time points and F_2BMet was extracted from various tissues. Figure 7 shows the pharmacokinetics in blood, tumor, muscle, and skin. The largest concentrations of F_2BMet, in terms of micrograms per gram of wet tissue, were observed in the liver, spleen, blood, and lungs, and are presented in the Supporting Information.

Photodynamic efficacy in vivo

The largest amounts of F_2BMet in the tumor (T) relative to muscle (M) tissue were observed 24 (T/M = 8) and 72 h (T/M = 16) post-i.v. administration. Thus, we made an exploratory study of PDT efficacy using DBA/2 mice with subcutaneously implanted S91 tumors for drug-to-light intervals (DLI) of 24 or 72 h. When a diameter of the tumor attained was approximately 5 mm, 2 mg kg^{-1} of F_2BMet was delivered in the tail vein, and after 24 or 72 h the tumors were illuminated with a light dose of 90 J cm^{-2} (diode laser at 750 nm, 90 mW). Figure 8 shows the time required for the tumors to attain the maximum diameter of 9.4 mm.

Table 3. Concentration of photosensitizers required to kill 50 or 90% of A549, PC-3, CT26, or HT-29 cells, in the dark or under a given laser-light (L) dose at 8 mW cm^{-2}.

	LD_{50} [μM]							LD_{90} [μM]					
	A549	PC-3		CT26		HT-29		A549	PC-3	CT26		HT-29	
L [J cm^{-2}]	6	6	0	1	6	0	1	6	6	1	6	1	6
Cl_2BOH	–	–	–	–	–	1058	–	–	19	–	–	–	46
Cl_2BEt	2.35	1.38	–	–	1.96	–	2.57	7.62	5.13	–	4.98	–	6.63
FBMet	0.17	0.13	–	–	0.37	–	–	0.47	0.52	–	1.31	–	0.93
F_2BMet	0.054	0.075	273	0.88	0.060	>200	0.37	0.15	0.38	5	0.71	0.6	–

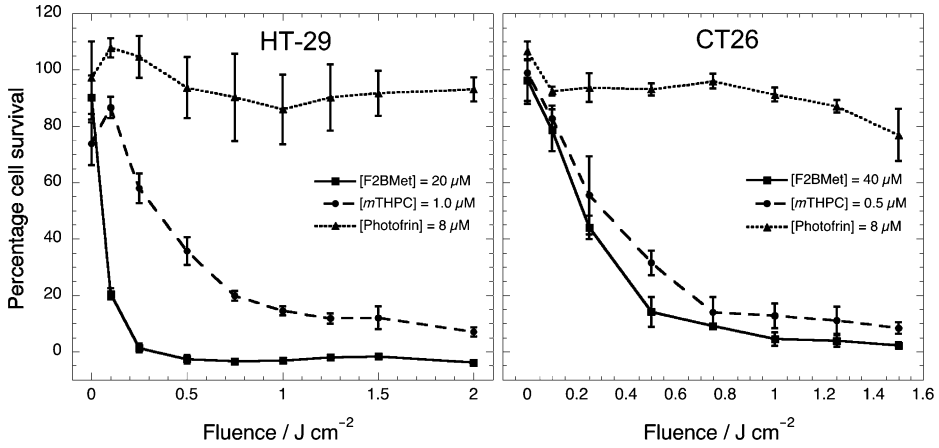

Figure 6. Survival fractions of HT-29 and CT26 cells incubated with F_2BMet, *m*THPC, or Photofrin below the onset of dark toxicity, as a function of the light dose.

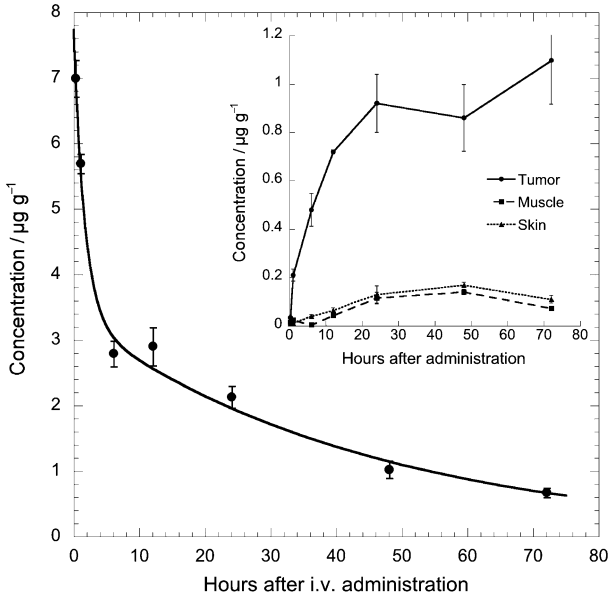

Figure 7. Pharmacokinetics and biodistribution of F_2BMet expressed as its concentration [$\mu g\,g^{-1}$] in wet tissue for the blood, tumor, surrounding skin, and muscle as a function of the time after i.v. administration of 2 $mg\,kg^{-1}$ to DBA/2 mice with S91-I3 tumors; each point represents the mean ± standard error of the mean (SEM) of three to four animals.

The illumination of the tumors with a single dose of 90 $J\,cm^{-2}$ led to the complete disappearance of the tumors in the following days. The protocol using DLI = 24 h leads to large edema and to the formation of a necrotic scab in the tumor region and in its vicinity in the first day after the treatment. A milder tumor response occurred in the first days after treatment with the DLI = 72 h protocol. In this case, necrotic changes were observed 3–4 days after the illumination and covered only the tumor region, without significant damage to the skin. The 24 h protocol proved more effective in delaying tumor regrowth, with a median tumor growth delay of 50 days with respect to control. A 50 days median tumor growth delay in this exploratory study with 2 $mg\,kg^{-1}$ and 90 $J\,cm^{-2}$ at DLI = 24 h must be regarded as a very promising starting point for future work.

Discussion

Empirical structure–activity relationships

Sulfonamide halogenated bacteriochlorins can meet the physicochemical properties of photosensitizers that are critical to the success of PDT but, in spite of their similarities, they exhibit in vitro phototoxicities that differ by a factor of 50. For example, 6 $J\,cm^{-2}$ at 749 nm require 7.6 μM of Cl_2BEt or 0.15 μM of F_2BMet to kill 90% of the A549 cells. The PDT efficacy increases in the sequence ClBEt < Cl_2BEt < FBMet < F_2BMet, and is not anticipated by the conventional structure–activity factors: ε_{745}, Φ_Δ, Φ_{pd}, or P_{OW}. It is possible that small differences in these properties combine to yield the distinct phototoxicities systematically observed under drug- and light-dose-dependent experiments, but the most striking observation is that F_2BMet has the lowest Φ_Δ and the highest phototoxicity. The remarkable phototoxicity of F_2BMet challenges the paradigm of PDT: the extent of type II reactions does explain relative phototoxicities and this highlights the relevance of type I reactions. Indeed, we have highlighted the role of charge-transfer interactions,[15] and the focus of structure–activity relationships in PDT is shifting from correlations with log P_{OW}[43] to the tuning of electronic properties.[9e]

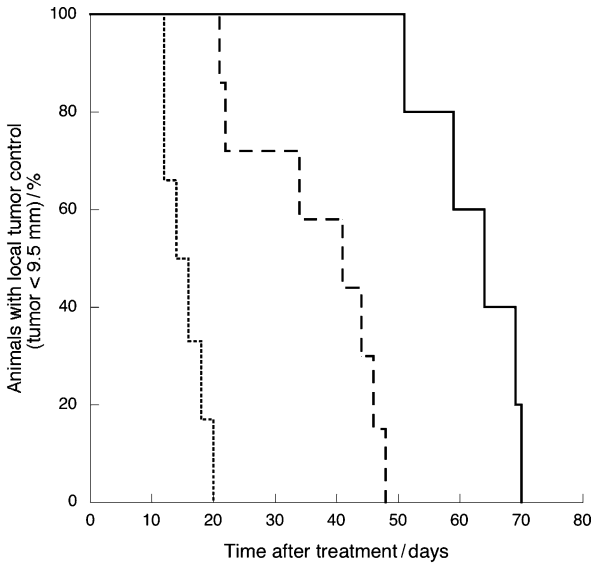

Figure 8. Kaplan–Meier plot of S91-I3 tumor regrowth in DBA/2 mice after PDT with 2 $mg\,kg^{-1}$ of F_2BMet i.v., followed by a light dose of 90 $J\,cm^{-2}$ at DLI = 24 (solid line) or 72 h (dashed line), with respect to the control group (dotted line).

The pattern of median tumor-regrowth delays (in days) after PDT with bacteriochlorins, ClBOH (27) < Cl_2BEt (44) < F_2BMet (50), is similar to that of in vitro phototoxicity.[16b,c] The biodistribution of F_2BMet at times longer than 6 h post-i.v. administration is comparable to that of other bacteriochlorins of the same family, and the differences in the early time points are related to the use of intraperitoneal (i.p.) administration in the earlier studies.[16b,c] The biodisponibility of F_2BMet after i.v. administration of 2 mg kg^{-1} is also similar to that of Cl_2BEt after i.p. injection of 10 mg kg^{-1} (0.9 versus 1.0 μg kg^{-1} in the tumor). Thus, S91-I3 tumor-regrowth delays in DBA/2 mice after PDT reflect the relative in vivo PDT efficacy and strengthen the need for a finer rationale for in vitro phototoxicity.

Dynamics enhance PDT

The actual rate constant for the deactivation of the triplet state of the photosensitizer in the encounter complex with molecular oxygen can only be obtained after correction for diffusion [Eq. (5)]:[44]

$$k_D = k_{-diff}\, k_q/(k_{diff} - k_q) \quad (5)$$

in which $k_{-diff} = k_{diff}/1$ M, but this is complicated by spin statistics. In the absence of charge-transfer interactions, $^1/_9\, k_{diff}$ should be used rather than k_{diff}, but in the presence of charge transfer both the singlet and triplet channels are active and $^4/_9\, k_{diff}$ should be used. The largest k_q/k_{diff} in ethanol was observed for FBMet and is between $^1/_9\, k_{diff}$ and $^4/_9\, k_{diff}$. Unfortunately, the correction for diffusion is dependent on the selection of the appropriate diffusion limit. Below we used a k_D value intermediate between these two limits in ethanol, 2.6 × 10^9 M^{-1} s^{-1}.

A large triplet deactivation rate constant (k_D), manifested by $k_q > {}^1/_9\, k_{diff}$, reveals the presence of significant charge transfer and should lead to a substantial fraction of oxygen-centered radicals. However, a large decomposition rate constant (k_d), manifested by $\Phi_{pd} > 10^{-5}$, should rapidly decompose the photosensitizer. Thus, the outcome of the {sensitizer···O_2} interaction in the encounter complex determines the nature of the ROS and their throughput. Ideally a photosensitizer should combine fast quenching (efficient formation of oxygen-centered radicals) with slow photodecomposition (ability to endure many cycles of ROS generation). This is found in F_2BMet.

Figure 9 shows that the relative PDT efficacy in vitro depends on the competition between ROS generation and degradation, k_D/k_d, for a constant rate of photon absorption (v_p). Appropriate offsets of the abscissa should be used for studies with different v_p, but this kinetic–activity relation is expected to be of great generality and provide a new rationale to guide the development of more efficient photosensitizers.

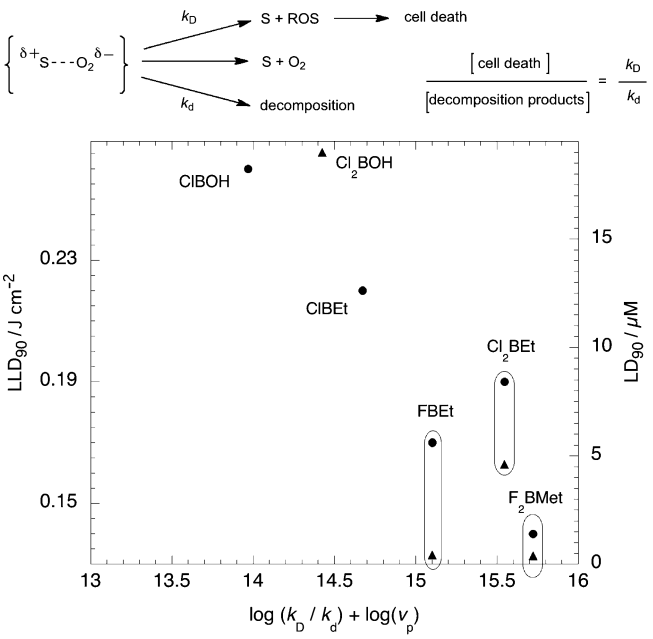

Figure 9. Top: reactive channels of the {sensitizer···O_2} interaction in the encounter complex. Bottom: Dependence of the light doses required to kill 90% of S91-I3 cells (LLD_{90}) or the photosensitizer doses required to kill 90% of PC3 cells on the balance between the reactive channels of halogenated sulfonamide bacteriochlorins.

Comparison with photosensitizers in clinical practice

F_2BMet has a much stronger absorption in the phototherapeutic window than Foscan (*m*THPC for injection, approved for clinical use) and Photofrin, with a comparable Φ_Δ but additionally generates superoxide ion. The Φ_{pd} of F_2BMet in PBS/methanol ($\Phi_{pd} = 1.0 \times 10^{-5}$) is smaller than that of Photofrin in PBS ($\Phi_{pd} = 5.4 \times 10^{-5}$).[45] The Φ_{pd} of F_2BMet drops to 6.9×10^{-7} in aerated ethanol, which is also smaller than that of Foscan in methanol, $\Phi_{pd} = 5 \times 10^{-6}$.[45,46] F_2BMet is generally more photostable than the photosensitizers in clinical use and reacts faster with molecular oxygen, which is consistent with its ability to generate various oxygen-centered radicals. The preference for ER localization observed for F_2BMet was also found for Foscan[47] and Photofrin.[48]

The comparison between these photosensitizers should be based on the ratio between dark cytotoxicity and phototoxicity, both defined for 50% of cell death, which was proposed as a therapeutic index (IP_{50}) of a photosensitizer [Eq. (6)]:[49]

$$IP_{50} = LD_{50dark}/LD_{50light} \quad (6)$$

The measurement of the dark and light toxicities gives the following IP_{50} values for CT26 cells: Photofrin (3.2), *m*THPC (81), and F_2BMet (311). For HT-29 cells the corresponding values are Photofrin (2.4), *m*THPC (21), and F_2BMet (> 540). The IP_{50} of F_2BMet is the highest of these photosensitizers under the same light dose and fluence rate. The Supporting Information presents the cytotoxicity studies used to obtain the IP_{50} values.

The pharmacokinetics of F_2BMet in mice exhibits a maximum concentration (C_{max}) in the blood shortly after i.v. administra-

tion and is well described by a two-compartment model with a distribution half-life of 1.1 h and a terminal half-life of 31 h. Plasma pharmacokinetics of Photofrin in human subjects follows a three-compartment model with half-lives of 2.08 min (distribution), 19.8 h, and 12.9 days.[50] Clinical pharmacokinetics of Foscan is unusual because C_{max} is observed approximately 24 h post-i.v. injection and then the elimination half-life is 45.5 h.[51] The elimination of F_2BMet is faster than those of Photofrin and Foscan and should reduce the skin photosensitivity after the treatment, often cited as the major inconvenience of PDT. Interestingly, PDT was more effective with DLI = 24 h than with DLI = 72 h, which correlates better with the amount of photosensitizer in the vascular compartment than in the tumor.

Conclusion

A library of tetraphenylbacteriochlorins with fluorine or chlorine atoms in the *ortho* positions of the phenyl groups was explored to select the "ideal" PDT photosensitizer because such bacteriochlorins can be economically synthesized,[10] exhibit a lower tendency to aggregate,[52] combine strong absorptions in the phototherapeutic window with efficient formation of long-lived triplet states,[14a,21b] bear electron-withdrawing groups that stabilize the macrocycle against oxidation,[53] and provide steric protection.[54] We found that the interaction between these bacteriochlorins and molecular oxygen led to superoxide ions and hydroxyl radicals in addition to singlet oxygen,[9d,15,55] and the combined effects of these ROS were remarkably efficient in the destruction of tumor cells.[7,16c] However, empirical correlations with lipophilicity or with electronic factors were insufficient to drive the last stage of PDT photosensitizer discovery.

A new path to discovery was opened with the finding that the strength of the {sensitizer···O_2} interaction is revealed by the quenching rate constant. Values of $k_q \geq 2\times10^9\,M^{-1}s^{-1}$ in ethanol indicate the ability to generate superoxide ion in addition to singlet oxygen, especially in hydroxylic solvents where the nascent superoxide ion is stabilized by hydrogen bonding. However, k_q depends on E^*_{ox} and lowering E_{ox} increases the photodecomposition quantum yield, Φ_{pd}. The bleaching of the photosensitizer becomes a limiting factor of PDT efficacy when $\Phi_{pd} > 10^{-5}$, which requires $E_{ox} > 0.8$ V versus SCE. The simultaneous fulfillment of the conditions $k_q \geq 2\times10^9\,M^{-1}s^{-1}$ in ethanol and $E_{ox} > 0.8$ V versus SCE should lead to photosensitizers that drive both type I and type II reactions without compromising photostability.

The dynamics of the interaction between the photosensitizer triplet state and oxygen determine both the nature of the ROS generated and the stability of the photosensitizer towards such ROS. F_2BMet attains a delicate balance between a high degree of charge transfer to oxygen and an adequate resistance to oxidation. It is an example of how the dynamics of the interaction between light, a photosensitizer, and oxygen can be tuned to increase tissue damage. Interestingly, in 1904 the term "photodynamic" was used to distinguish PDT from the physicochemical processes occurring in the emulsions of photographic films.[1] Over one century later, dynamics provide a rationale to select the best photosensitizers for PDT.

Experimental Section

5,10,15,20-Tetrakis(2,6-difluoro-3-*N*-methylsulfamoylphenyl) porphyrin (F_2PMet)

A mixture of F_2P[14a] and chlorosulfonic acid (1:680) was added to a round-bottomed flask equipped with a magnetic stirrer. The mixture was kept at 110 °C until the tetrachlorosulfonylated compound was observed by TLC. After cooling, dichloromethane was added, and the excess amount of acid was removed with a saturated solution of sodium bicarbonate in water. After evaporation the crude was redissolved in dichloromethane and a solution of methylamine in THF (2.0 M) was added. The reaction was kept at 20 °C until full consumption of the starting materials. Finally the solution was extracted with HCl (0.1 M) and water. After chromatography with silica gel (dichloromethane/ethyl acetate), F_2PMet was obtained in 70% yield. ^{1}H NMR (400 MHz, $CDCl_3$): $\delta = -2.84$ (s, 2H), 2.87–2.90 (m, 12H), 4.73 (m, 4H), 7.45–7.54 (m, 4H), 8.42–8.49 (m, 4H), 8.84 ppm (s, 8H); ^{19}F NMR (376.5 MHz, $CDCl_3$): $\delta = -104.17$ to -104.11 (m, 4F); -98.54 to -98.49 ppm (m, 4F); HRMS (ESI-FIA-TOF): *m/z* calcd for $C_{48}H_{35}F_8N_8O_8S_4$: 1131.1327; found: 1131.1328 [M+H$^+$]; elemental analysis calcd (%) for $C_{48}H_{34}F_8N_8O_8S_4{\cdot}H_2O$: calcd C 50.17, H 3.16, N 9.75, S 11.16; found: C 50.47, H 3.18, N 9.39, S 10.94.

5,10,15,20-Tetrakis(2,6-difluoro-3-*N*-methylsulfamoylphenyl) bacteriochlorin (F_2BMet)

This bacteriochlorin was prepared on the multigram scale with our solvent-free method.[13] A mixture of F_2PMet and *p*-toluenosulfonylhydrazide (1:40) was ground in a Schlenk tube and then evacuated with a vacuum pump. Next, the reactor was heated at 140 °C for 60 min, and then brought back to room temperature. After chromatography with silica gel (dichloromethane/ethyl acetate), F_2BMet was obtained in 85% yield. ^{1}H NMR (400 MHz, $CDCl_3$): $\delta = -1.38$ (s, 2H), 2.77–2.84 (m, 12H), 4.06 (s, 8H), 4.65–4.71 (m, 4H), 7.39–7.43 (m, 4H), 8.00–8.03 (m, 4H), 8.24–8.29 ppm (m, 4H); ^{19}F NMR (376.5 MHz, $CDCl_3$): $\delta = -105.09$ to -104.95 (m, 4F); -99.48 to -99.37 ppm (m, 4F); HRMS (ESI-FIA-TOF): *m/z* calcd for $C_{48}H_{39}F_8N_8O_8S_4$: 1135.1640; found: 1135.1612 [M+H$^+$]; elemental analysis calcd (%) for $C_{48}H_{34}F_8N_8O_8S_4{\cdot}H_2O$: C 50.00, H 3.50, N 9.72, S 11.12; found: C 49.88, H 3.47, N 9.38, S 10.94.

Other porphyrin derivatives

The other photosensitizers employed in this study were available from previous studies or were synthesized according to the literature.[10,13] *m*THPP was synthesized by means of the nitrobenzene method,[56] and *m*THPC was synthesized with our solvent-free method.[13] Details are given in the Supporting Information.

Animals and tumor model

The animal model used for dark toxicity, biodistribution, and pharmacokinetic studies was the DBA mouse bearing the Cloudman S91-I3 melanoma. Following approval by the Jagiellonian University Committee for Ethics of Experiments on Animals (decision no. 89/2008 from 11 December 2008 and no. 11/2011, 23 February 2011), mice (20–30 g) from the Animal House of the Polish Academy of Science Medical Research Center (Warsaw, Poland) enrolled

in the experiments were kept on a standard laboratory diet with free access to drinking water. The S91 cells were cultured in vitro and after a subcutaneous inoculation of 1×10^6 cells into the right flank, tumors were induced in 100% of mice. The tumors grew exponentially and displayed only a little size scatter between animals.

Photodynamic therapy

S91-I3 tumors were grown in DBA/2 mice as described above. The treatment was initiated when the tumor attained at least 5 mm in one diameter in each animal. A dose of 2 mg kg^{-1} of F_2BMet was injected in the tail vein on the day the tumors reached the treatment size. At 24 or 72 h post-injection, the mice were anesthetized with ketamine and xylazine, and restrained in plastic holders, then treated with the Hamamatsu laser described above, at a fluence rate of 80–90 mW cm^{-2} for 20 min. The mice (5–7 mice per group in three groups (not treated, treated with light, treated with light and photosensitizer) were checked daily. The tumors were measured using two radicular diameters L (length) and W (width) and the volumes were calculated using the formula $V=L\times W^2/2$.

Acknowledgements

This work was supported by the Fundação para a Ciência e a Tecnologia (FCT) grant PEst-OE/QUI/UI0313/2014 and ERA Chemistry (PL-grant no. 60 303, The National Centre for Research and Development, PT-grant no. 0002/2008, FCT-FEDER). J.M.D. thanks the Ministry of Science and Higher Education (Poland) for an Iuventus Plus grant (no. IP2011009471). E.F.F.S. thank FCT for a PhD grant SFRH/BD/46658/2008. We thank Nuno Gonçalves, Gonçalo Costa, Carlos Monteiro, and Vanessa Simões for assistance with the synthesis, and Luisa Cortes for the confocal microscopy.

Keywords: charge transfer · cytotoxicity · photophysics · porphyrinoids · singlet oxygen

[1] T. J. Dougherty, C. J. Gomer, B. W. Henderson, G. Jori, D. Kessel, M. Korbelik, J. Moan, Q. Peng, *J. Natl. Cancer Inst.* **1998**, *90*, 889–905.

[2] a) P. Agostinis, K. Berg, K. A. Cengel, T. H. Foster, A. W. Girotti, S. O. Golinick, S. M. Hahn, M. R. Hamblin, A. Juzeniene, D. Kessel, M. Korbelik, J. Moan, P. Mroz, D. Nowis, J. Piette, B. C. Wilson, J. Golab, *CA Cancer J. Clin.* **2011**, *61*, 250–281; b) S. Yano, S. Hirohara, M. Obata, Y. Hagiya, S.-I. Ogura, A. Ikeda, H. Kataoka, M. Tanaka, T. Joh, *J. Photochem. Photobiol. C* **2011**, *12*, 46–67.

[3] P. Mroz, A. Szokalska, M. X. Wu, M. R. Hamblin, *PLoS ONE* **2010**, *5*, e15194.

[4] A. Master, M. Livingstone, A. S. Gupta, *J. Controlled Release* **2013**, *168*, 88–102.

[5] a) E. D. Sternberg, D. Dolphin, *Tetrahedron* **1998**, *54*, 4151–4202; b) G. Jori, in *Photodynamic Therapy: Basic and Preclinical Aspects, Vol.* (Eds.: W. M. Horspool, F. Lenci), CRC, Boca Raton, **2004**, Ch. 146. 1–10; c) M. R. Detty, S. L. Gibson, S. J. Wagner, *J. Med. Chem.* **2004**, *47*, 3897–3915; d) M. Ethirajan, C. Saenz, A. Gupta, M. P. Dobhal and R. K. Pandey, in *Photosensitizers for Photodynamic Therapy and Imaging, Vol.* (Eds.: M. R. Hamblin, P. Mroz), Arthech House, Norwood, **2008**, Ch. 2, pp. 13–40; e) L. G. Arnaut, S. J. Formosinho, *Pure Appl. Chem.* **2013**, *85*, 1389–1403.

[6] a) I. J. MacDonald, T. J. Dougherty, *J. Porphyrins Phthalocyanines* **2001**, *5*, 105–129; b) D. E. Dolmans, D. Fukumura, R. K. Jain, *Nat. Rev. Cancer* **2003**, *3*, 380–387.

[7] J. M. Dabrowski, L. G. Arnaut, M. M. Pereira, K. Urbanska, S. Simoes, G. Stochel, L. Cortes, *Free Radical Biol. Med.* **2012**, 1188–1200.

[8] a) D. V. Krysko, A. D. Garg, A. Kaczmarek, O. Krysko, P. Agostinis, P. Vandenabeele, *Nature Rev. Cancer* **2012**, *12*, 860–875; b) A. D. Garg, D. V. Krysko, T. Verfaillie, A. Kaczmarek, G. B. Ferreira, T. Marysael, N. Rubio, M. Firczuk, C. Mathieu, A. J. M. Roebroek, W. Annaert, J. Golab, P. de Witte, P. Vandenabeele, P. Agostinis, *EMBO J.* **2012**, *31*, 1062–1079.

[9] a) A. Gryshuk, Y. Chen, L. N. Goswami, S. Pandey, J. R. Missert, T. Ohulchanskyy, W. Potter, P. N. Prasad, A. Oseroff, R. K. Pandey, *J. Med. Chem.* **2007**, *50*, 1754–1767; b) Y.-Y. Huang, P. Mroz, T. Zhiyentayev, S. K. Sharma, T. Balasubramanian, C. Ruzié, M. Krayer, D. Fan, K. E. Borbas, E. Yang, H. L. Kee, C. Kirmaier, J. R. Diers, D. F. Bocian, D. Holten, J. S. Lindsey, M. R. Hamblin, *J. Med. Chem.* **2010**, *53*, 4018–4027; c) L. G. Arnaut, *Adv. Inorg. Chem.* **2011**, *63*, 187–233; d) E. Yang, J. R. Diers, Y.-Y. Huang, M. R. Hamblin, J. S. Lindsey, D. F. Bocian, D. Holten, *Photochem. Photobiol.* **2013**, *89*, 605–618.

[10] M. M. Pereira, C. J. P. Monteiro, A. V. C. Simoes, S. M. A. Pinto, A. R. Abreu, G. F. F. Sa, E. F. F. Silva, L. B. Rocha, J. M. Dabrowski, S. J. Formosinho, S. Simoes, L. G. Arnaut, *Tetrahedron* **2010**, *66*, 9545–9551.

[11] a) Y. Vakrat-Haglili, L. Weiner, V. Brumfeld, A. Brandis, Y. Salomon, B. McIlroy, B. C. Wilson, A. Pawlak, M. Rozanowska, T. Sarna, A. Scherz, *J. Am. Chem. Soc.* **2005**, *127*, 6487–6497; b) O. Mazor, A. Brandis, V. Plaks, E. Neumark, V. Rosenbach-Belkin, Y. Salomon, A. Scherz, *Photochem. Photobiol.* **2005**, *81*, 342–351; c) S. Chevalier, M. Anidjar, E. Scarlata, L. Hamel, A. Scherz, H. Ficheux, N. Borenstein, L. Fiette, M. Elhilali, *J. Urol.* **2011**, *186*, 302–309; d) A. Azzouzi, E. Barret, A. Villers, *J. Urol.* **2011**, *185*, e718–719.

[12] a) M. Taniguchi, D. L. Cramer, A. D. Bhise, H. L. Kee, D. F. Bocian, D. Holten, J. S. Lindsey, *New J. Chem.* **2008**, *32*, 947–958; b) T. G. Minehan, L. Cook-Blumberg, Y. Kishi, M. R. Prinsep, R. E. Moore, *Angew. Chem.* **1999**, *111*, 975–977; *Angew. Chem. Int. Ed.* **1999**, *38*, 926–928; c) W. Wang, Y. Kishi, *Org. Lett.* **1999**, *1*, 1129–1132; d) H.-J. Kim, J. S. Lindsey, *J. Org. Chem.* **2005**, *70*, 5475–5486; e) C. Ruzié, M. Krayer, T. Balasubramanian, J. S. Lindsey, *J. Org. Chem.* **2008**, *73*, 5806–5820; f) M. Krayer, T. Balasubramanian, C. Ruzié, M. Ptaszek, D. L. Cramer, M. Taniguchi, J. S. Lindsey, *J. Porphyrins Phthalocyanines* **2009**, *13*, 1098–1110; g) M. Krayer, M. Ptaszek, H.-J. Kim, K. R. Meneely, D. Fan, K. Seor, J. S. Lindsey, *J. Org. Chem.* **2010**, *75*, 1016–1039; h) Y.-Y. Huang, T. Balasubramanian, E. Yang, D. Luo, J. R. Diers, D. F. Bocian, J. S. Lindsey, D. Holten, M. R. Hamblin, *ChemMedChem* **2012**, *7*, 2155–2167.

[13] M. M. Pereira, A. A. Abreu, N. P. F. Goncalves, M. J. F. Calvete, A. V. C. Simões, C. J. P. Monteiro, L. G. Arnaut, M. E. Eusébio, J. Canotilho, *Green Chem.* **2012**, *14*, 1666–1672.

[14] a) M. Pineiro, A. M. d. A. R. Gonsalves, M. M. Pereira, S. J. Formosinho, L. G. Arnaut, *J. Phys. Chem. A* **2002**, *106*, 3787–3795; b) M. M. Pereira, C. J. P. Monteiro, A. V. C. Simões, S. M. A. Pinto, L. G. Arnaut, G. F. F. Sá, E. F. F. Silva, L. B. Rocha, S. Simões, S. J. Formosinho, *J. Porphyrins Phthalocyanines* **2009**, *13*, 567–573.

[15] E. F. F. Silva, C. Serpa, J. M. Dabrowski, C. J. P. Monteiro, L. G. Arnaut, S. J. Formosinho, G. Stochel, K. Urbanska, S. Simoes, M. M. Pereira, *Chem. Eur. J.* **2010**, *16*, 9273–9286.

[16] a) J. M. Dabrowski, L. G. Arnaut, M. M. Pereira, C. J. P. Monteiro, K. Urbanska, S. Simões, G. Stochel, *ChemMedChem* **2010**, *5*, 1770–1780; b) J. M. Dabrowski, K. Urbanska, L. G. Arnaut, M. M. Pereira, A. R. Abreu, S. Simões, G. Stochel, *ChemMedChem* **2011**, *6*, 465–475; c) J. M. Dabrowski, L. G. Arnaut, M. M. Pereira, K. Urbanska, G. Stochel, *MedChemComm* **2012**, *3*, 502–505.

[17] P. Joshi, M. Ethirajan, L. N. Goswami, A. Srivatsan, J. R. Missert, R. K. Pandey, *J. Org. Chem.* **2011**, *76*, 8629–8640.

[18] M. Pineiro, M. M. Pereira, A. M. d. A. R. Gonsalves, L. G. Arnaut, S. J. Formosinho, *J. Photochem. Photobiol. A* **2001**, *138*, 147–157.

[19] A. V. C. Simões, A. Adamowicz, J. M. Dabrowski, M. J. F. Calvete, A. A. Abreu, G. Stochel, L. G. Arnaut, M. M. Pereira, *Tetrahedron* **2012**, *68*, 8767–8772.

[20] C. J. P. Monteiro, M. M. Pereira, S. M. A. Pinto, A. V. C. Simões, G. F. F. Sá, L. G. Arnaut, S. J. Formosinho, S. Simões, M. F. Wyatt, *Tetrahedron* **2008**, *64*, 5132–5138.

[21] a) M. Pineiro, A. L. Carvalho, M. M. Pereira, A. M. d. A. R. Gonsalves, L. G. Arnaut, S. J. Formosinho, *Chem. Eur. J.* **1998**, *4*, 2299–2307; b) E. G. Azenha, A. C. Serra, M. Pineiro, M. M. Pereira, J. Seixas de Melo, L. G. Arnaut, S. J. Formosinho, A. M. d. A. R. Gonsalves, *Chem. Phys.* **2002**, *280*, 177–190.

[22] C. K. Chang, L. K. Hanson, P. F. Richardson, R. Young, J. Fajer, *Proc. Natl. Acad. Sci. USA* **1981**, *78*, 2652 – 2656.
[23] a) C. J. P. Monteiro, J. Pina, M. M. Pereira, L. G. Arnaut, *Photochem. Photobiol. Sci.* **2012**, *11*, 1233 – 1238; b) E. F. F. Silva, F. A. Schaberle, C. J. P. Monteiro, J. M. Dabrowski, L. G. Arnaut, *Photochem. Photobiol. Sci.* **2013**, *12*, 1187 – 1192.
[24] Y.-J. Tu, H. C. Chenh, I. Chao, C.-R. Cho, R.-J. Cheng, Y. O. Su, *J. Phys. Chem. A* **2012**, *116*, 1632 – 1637.
[25] J. M. Dabrowski, M. M. Pereira, L. G. Arnaut, C. J. P. Monteiro, A. F. Peixoto, A. Karocki, K. Urbanska, G. Stochel, *Photochem. Photobiol.* **2007**, *83*, 897 – 903.
[26] G. S. Wilson, G. Peychal-Heiling, *Anal. Chem.* **1971**, *43*, 550 – 556.
[27] R. Bonnett, P. Charlesworth, B. D. Djelal, D. J. McGarvey, T. G. Truscott, *J. Chem. Soc. Perkin Trans. 2* **1999**, 325 – 328.
[28] R. W. Redmond, J. N. Gamlin, *Photochem. Photobiol.* **1999**, *70*, 391 – 475.
[29] C. Tanielian, C. Wolff, M. Esch, *J. Phys. Chem.* **1996**, *100*, 6555 – 6560.
[30] F. A. Schaberle, R. M. D. Nunes, M. Barroso, C. Serpa, L. G. Arnaut, *Photochem. Photobiol. Sci.* **2010**, *9*, 812 – 822.
[31] A. Kozyrev, M. Ethirajan, P. Chen, K. Ohkubo, B. C. Robinson, K. M. Barkigia, S. Fukuzumi, K. M. Kadish, R. K. Pandey, *J. Org. Chem.* **2012**, *77*, 10260 – 10271.
[32] T. N. Rao, B. V. Sarada, D. A. Tryk, A. Fujishima, *J. Electroanal. Chem.* **2000**, *491*, 175 – 181.
[33] L. Fotouhi, M. Fatollahzadeh, M. M. Heravi, *Int. J. Electrochem. Sci.* **2012**, *7*, 3919 – 3928.
[34] C. Huang, M. Tian, Y. Yang, F. Guo, M. Wang, *J. Electroanal. Chem.* **1989**, *272*, 179 – 184.
[35] a) J. Chevalet, F. Rouelle, L. Gierst, J. P. Lambert, *Electroanal. Chem. Interfac. Electrochem.* **1972**, *39*, 201 – 216; b) W. H. Koppenol, D. M. TStanbury, P. L. Bounds, *Free Radical Biol. Med.* **2010**, *49*, 317 – 322.
[36] a) A. Garner, F. Wilkinson, *Chem. Phys. Lett.* **1977**, *45*, 432 – 435; b) F. Wilkinson, A. A. Abdel-Shafi, *J. Phys. Chem. A* **1997**, *101*, 5509 – 5516; c) C. Schweitzer, R. Schmidt, *Chem. Rev.* **2003**, *103*, 1685 – 1757.
[37] A. A. Abdel-Shafi, F. Wilkinson, *Phys. Chem. Chem. Phys.* **2002**, *4*, 248 – 254.
[38] S. L. Murov, I. Carmichael and G. L. Hug, *Handbook of Photochemistry*, Marcel Dekker, New York, **1993**.
[39] G. Helmlinger, F. Yuan, M. Dellian, R. K. Jain, *Nat. Med.* **1997**, *3*, 177 – 182.
[40] P. Mroz, J. Bhaumik, D. K. Dogutan, Z. Aly, Z. Kamal, L. Khalid, H. L. Kee, D. F. Bocian, D. Holten, J. S. Lindsey, M. R. Hamblin, *Cancer Lett.* **2009**, *282*, 63 – 76.
[41] P. Nowak-Sliwinska, A. Karocki, M. Elas, A. Pawlak, G. Stochel, K. Urbanska, *Biochem. Biophys. Res. Commun.* **2006**, *349*, 549 – 555.
[42] B. Cunderlíková, O. Kaalhus, R. Cunderlík, A. Mateásik, J. Moan, M. Kongshaug, *Photochem. Photobiol.* **2004**, *79*, 242 – 247.
[43] B. W. Henderson, D. A. Bellnier, W. R. Greco, S. Amarnath, R. K. Pandey, L. A. Vaughan, K. R. Weishaupt, T. J. Dougherty, *Cancer Res.* **1997**, *57*, 4000 – 4007.
[44] R. Schmidt, F. Shafii, C. Schweitzer, A. Abdel-Shafi, F. Wilkinson, *J. Phys. Chem. A* **2001**, *105*, 1811 – 1817.
[45] R. Bonnett, G. Martinez, *Tetrahedron* **2001**, *57*, 9513 – 9547.
[46] R. Bonnett, B. D. Djelal, P. A. Hamilton, G. Martinez, F. Wierrani, *J. Photochem. Photobiol. B* **1999**, *53*, 136 – 143.
[47] M.-H. Teiten, L. Bezdetnaya, P. Morlière, R. Santus, F. Guillemin, *Br. J. Cancer* **2003**, *88*, 146 – 152.
[48] Y.-J. Hsieh, J.-S. Yu, P.-C. Lyu, *J. Cell. Biochem.* **2010**, *111*, 821 – 833.
[49] J. Berlanda, T. Kiesslich, V. Engelhardt, B. Krammer, K. Plaetzer, *J. Photochem. Photobiol. B* **2010**, *100*, 173 – 180.
[50] S. P. Pereira, L. Ayaru, R. Ackroyd, D. Mitton, G. Fullarton, M. M. Zammit, Z. Grzebieniak, H. Messmann, M.-A. Ortner, L. Gao, M. M. Trinh, J. Spénard, *Aliment. Pharmacol. Ther.* **2010**, *32*, 821 – 827.
[51] A. M. Ronn, M. Nouri, L. A. Lofgren, B. M. Steinberg, A. Westerborn, T. Windhal, M. J. Shikowitz, A. L. Abramson, *Lasers Med. Sci.* **1996**, *11*, 267 – 272.
[52] T. P. G. Sutter, R. Rahimi, P. Hambright, J. C. Bommer, M. Kiumar, P. Neta, *J. Chem. Soc. Faraday Trans.* **1993**, *89*, 495 – 502.
[53] S. I. Yang, J. Seth, J.-P. Strachan, S. Gentemann, D. Kim, D. Holten, J. S. Lindsey, D. F. Bocian, *J. Porphyrins Phthalocyanines* **1999**, *3*, 117 – 147.
[54] A. M. S. Silva, M. G. P. M. S. Neves, R. R. L. Martins, J. A. S. Cavaleiro, T. Boschi, P. Tagliatesta, *J. Porphyrins Phthalocyanines* **1998**, *2*, 45 – 51.
[55] E. F. F. da Silva, B. W. Pedersen, T. Breitenbach, R. Toftegaard, M. K. Kuimova, L. G. Arnaut, P. R. Ogilby, *J. Phys. Chem. B* **2012**, *116*, 445 – 461.
[56] A. M. d. A. Rocha Gonsalves, J. M. T. B. Varejao, M. M. Pereira, *J. Heterocycl. Chem.* **1991**, *28*, 635 – 640.

Received: October 28, 2013
Published online on March 18, 2014